Performance of Ordered-Subset Reconstruction Algorithms Under Conditions of Extreme Attenuation and Truncation in Myocardial SPECT

David S. Lalush and Benjamin M.W. Tsui

Departments of Biomedical Engineering and Radiology, University of North Carolina at Chapel Hill, Chapel Hill, North Carolina

We studied the bias and variance characteristics of the ordered-subset expectation maximization (OSEM) and rescaled block-iterative EM (RBIEM) iterative reconstruction algorithms in myocardial SPECT under extreme, but realistic, conditions. **Methods:** We used the 2-dimensional mathematic cardiac torso phantom to simulate 2 patient anatomies: a large male with a raised diaphragm and a female with large breast size, approximating extreme cases of attenuation conditions found in the clinic. For each anatomy, realistic ^{201}Tl projection data were simulated for a 180° acquisition arc. Three cases of truncation for a 90°-configured dual detector system were simulated: no truncation, moderate truncation, and extreme truncation. For each case, an ensemble of 250 noise simulations was generated, and each noisy dataset was reconstructed with the OSEM and RBIEM algorithms. The reconstructions modeled only the effects of nonuniform attenuation and used a range of subset configurations. Over the ensemble, we computed means and variances of activity in 8 regions of interest (ROIs) in the heart as a function of iteration. **Results:** Under conditions of no truncation and moderate truncation, the results from OSEM and RBIEM were very close to those from maximum-likelihood EM (MLEM); in all cases, the difference in ROI means was <2.5%. For extreme truncation, the errors increased to as much as 11% with OSEM, but these were no greater than the errors for MLEM under the same conditions. The OSEM algorithm with 2 views per subset was found to result in much higher variance of ROI estimates for the same bias as compared with RBIEM or OSEM with 4 or more views per subset. **Conclusion:** The OSEM and RBIEM algorithms are at least as robust to highly attenuating patients and truncation as MLEM algorithm and can be adequate substitutes for MLEM, even in extreme cases. Clinical users should apply the smallest number of subsets that can be accommodated by allowable processing time to reduce image noise and variance in quantitative estimates.

Key Words: iterative reconstruction; attenuation compensation; myocardial SPECT

J Nucl Med 2000; 41:737–744

Iterative reconstruction algorithms for nuclear medicine are finding wider use in both research and commercial products, as procedures for nonuniform attenuation compensation become more commonplace (*1–3*). The lineage of the most widely used iterative reconstruction algorithms can be traced back to the maximum-likelihood expectation maximization (MLEM) algorithm (*4,5*). This algorithm has a strong theoretic basis and has been widely studied, so that its noise and convergence properties are well known (*6–12*). Unfortunately, in the past, reaching a usable solution with the algorithm required too many iterations to be practical for use in a clinical product.

Ordered-subset algorithms, which are related to but much faster than MLEM, have quickly become the dominant iterative reconstruction procedures in both PET and SPECT in recent years. These algorithms include the ordered-subset EM (OSEM) algorithm (*13*) and the rescaled block-iterative EM (RBIEM) algorithm (*14*). The OSEM algorithm has been chosen both for its impressive speed, usually requiring fewer than 5 iterations to reach a usable solution, and for its relative simplicity of implementation.

Unfortunately, these algorithms are widely misunderstood. Because of their close relationship in form with MLEM, it is frequently assumed that they seek the maximum-likelihood solution and are simply faster versions of MLEM. No general proof has been found that this is the case. In fact, there is currently no general proof that these algorithms will converge to any particular solution at all. They are poorly named, because they are not actually EM algorithms and do not maximize any function. Although the general experience with OSEM has been very good and it appears to closely emulate the results of MLEM, to date the only way to prove that these algorithms are accurate and effective is through careful empiric study.

In previous simulation studies of ^{201}Tl myocardial SPECT using the 3-dimensional mathematical cardiac torso (MCAT) phantom (*15*), we found that both OSEM and RBIEM gave image estimates that were very close to those from MLEM in the region of the heart. However, in the case of a medium-sized male phantom with data acquired over a 180° arc, OSEM reconstructions overestimated intensity in a liver region of interest (ROI) by 4%–6% compared with MLEM. We speculated that the error in the liver may be an

Received Feb. 8, 1999; revision accepted Aug. 9, 1999.

For correspondence or reprints contact: David S. Lalush, PhD, Department of Biomedical Engineering, CB 7575, 152 MacNider Hall, University of North Carolina at Chapel Hill, Chapel Hill, NC 27599-7575.

attenuation effect and could result in quantitative errors in the heart in highly attenuating patients. Also, we observed that OSEM appeared to be sensitive to errors in the model of the projection process, hypothesizing that truncation of emission data might create inaccuracies.

In this study, we seek to evaluate the performance of OSEM and RBIEM under extreme but realistic conditions of attenuation and truncation to determine if they truly are able to give results similar to MLEM, but faster. Also, we examine the effects of changing subset configurations on convergence and accuracy of ROI estimation in myocardial perfusion SPECT.

MATERIALS AND METHODS

Algorithms

The OSEM reconstruction algorithm (*13*) can be written as:

$$x_i^{new} = \frac{x_i^{old}}{\sum_{j \in S_n} c_{ji}} \sum_{j \in S_n} c_{ji} \frac{p_j}{\sum_k c_{jk} x_k^{old}}, \quad \text{Eq. 1}$$

where x_i represents the estimated intensity at pixel i, p_j represents the measured events in projection bin j, and c_{ji} represents the relative contribution of pixel i to the measurement in projection bin j. The c elements may model nonuniform attenuation, detector response (*16,17*), or scatter (*18,19*). The old and new superscripts indicate the previous and new iterated estimates, respectively. The backprojection (summation over bins) is done for a subset S_n of the projection bins, usually those corresponding to a particular set of views. After an iterated update is performed for 1 subset, another update is performed using another subset of the measured projection data, and so on, until all the projection data have been used. Then the process repeats again starting with the first subset. In this article, we refer to a single update from a particular subset as a subiteration, and the set of updates using all the projection data once as an iteration.

The RBIEM algorithm (*14*) can be written:

$$x_i^{new} = x_i^{old} + t_n^{-1} \frac{x_i^{old}}{\sum_j c_{ji}} \sum_{j \in S_n} c_{ji} \left[\frac{p_j}{\sum_k c_{jk} x_k^{old}} - 1 \right]; \quad t_n = \max_i \left(\frac{\sum_{j \in S_n} c_{ji}}{\sum_j c_{ji}} \right), \quad \text{Eq. 2}$$

where the parameter t_n is determined for each subset by maximizing over all pixels the ratio of subset weighting factors to total weighting factors as shown. Note that both OSEM and RBIEM reduce to MLEM when a single subset is chosen.

Phantoms

The 3-dimensional MCAT phantom (*20*) was used as the basis for the phantoms used in this work. It is a geometric representation of a simulated patient's anatomy using ellipsoids, cylinders, and other objects. By manipulating the geometric objects, it is possible to simulate patients of different body types. From a defined anatomy, we generate both emission distributions and attenuation distributions for simulation of SPECT data. This gives realistic patientlike SPECT data but with the advantage of having the true activity distribution known for use in quantitative comparisons.

Two of the most highly attenuating anatomies from the MCAT population were used, as shown in Figure 1 (*21*). These include a large male with a raised liver and a female with large breast size. These phantom anatomies were based on actual patient scans (*21*); therefore, although extreme, they are not out of the realm of possibility. For purposes of simulation, both phantoms were generated on a 128 × 128 voxel grid with cubic voxels of side length 3.125 mm.

Simulation

Parallel projection data from each of the 2 phantoms was simulated to model a typical ^{201}Tl acquisition in our clinic. Projections were computed using a rotation-based projection subroutine that realistically models the effects of attenuation, collimator–detector response (low-energy general-purpose collimator), and scatter (*18*). The simulation modeled data acquisition for 64 views over the 180° arc from 45° right anterior oblique to 45° left posterior oblique at a radius of rotation of 23 cm. With the 90°-configured dual-detector system, this models a 90° rotation of the gantry. Each projection consisted of 128 × 128 square projection bins of side length 3.125 mm. After the projections were computed, the bins were collapsed to 6.25 mm to simulate the effects of sampling.

To simulate truncation, we modeled 3 different camera sizes for a 90°-configured dual-detector system. The camera sizes modeled were 43 cm or greater, referred to as no truncation; 36 cm, referred to as moderate truncation; and 30 cm, referred to as extreme truncation. The extreme truncation case cut off a significant portion of the right lung and liver, but the heart was not truncated in any view. Note that truncation was applied only to the emission data sets; the transmission maps were assumed to be complete in all 3 cases.

Poisson noise was simulated to approximate the typical count level for a patient dose of 74 MBq (2 mCi) ^{201}Tl, based on patient scans from our clinic. The resulting projection data had total count levels of 65,000–72,000 counts per 6.25-mm slice through the left ventricle. Poisson noise was simulated using the noise-free projection values as mean values. For each anatomy–truncation combination, the Poisson-noise simulation process was repeated 250 times, each with a different random number seed. Thus, an ensemble of 250 independent noisy data sets was generated for each case. A single noisy data set is referred to as a noise realization.

Reconstruction

Each noise realization for each case was reconstructed using OS-EM with 2 and 4 views per subset and using RBIEM with 2 views per subset, saving each iteration up to 20. For comparison, we reconstructed the full set of noise realizations using MLEM for the cases of no truncation and extreme truncation, saving every 10 iterations up to 200. To study the effects of changing the number of views per subset, we reconstructed the full set of noise realizations for the case of no truncation using OSEM and RBIEM at 2, 4, 8, and 16 views per subset. In all cases, subsets were configured to obtain the maximum angular difference between successive subsets.

Reconstructions modeled only the effects of nonuniform attenuation. The attenuation maps used in the reconstruction were collapsed from the original phantoms to a voxel size of 6.25 mm, and then convolved with a gaussian blur of full width at half maximum of approximately 1 cm to simulate imperfect resolution of the transmission measurement. No noise was applied to the attenuation maps so as not to introduce additional noise variations beyond those in the emission data simulations.

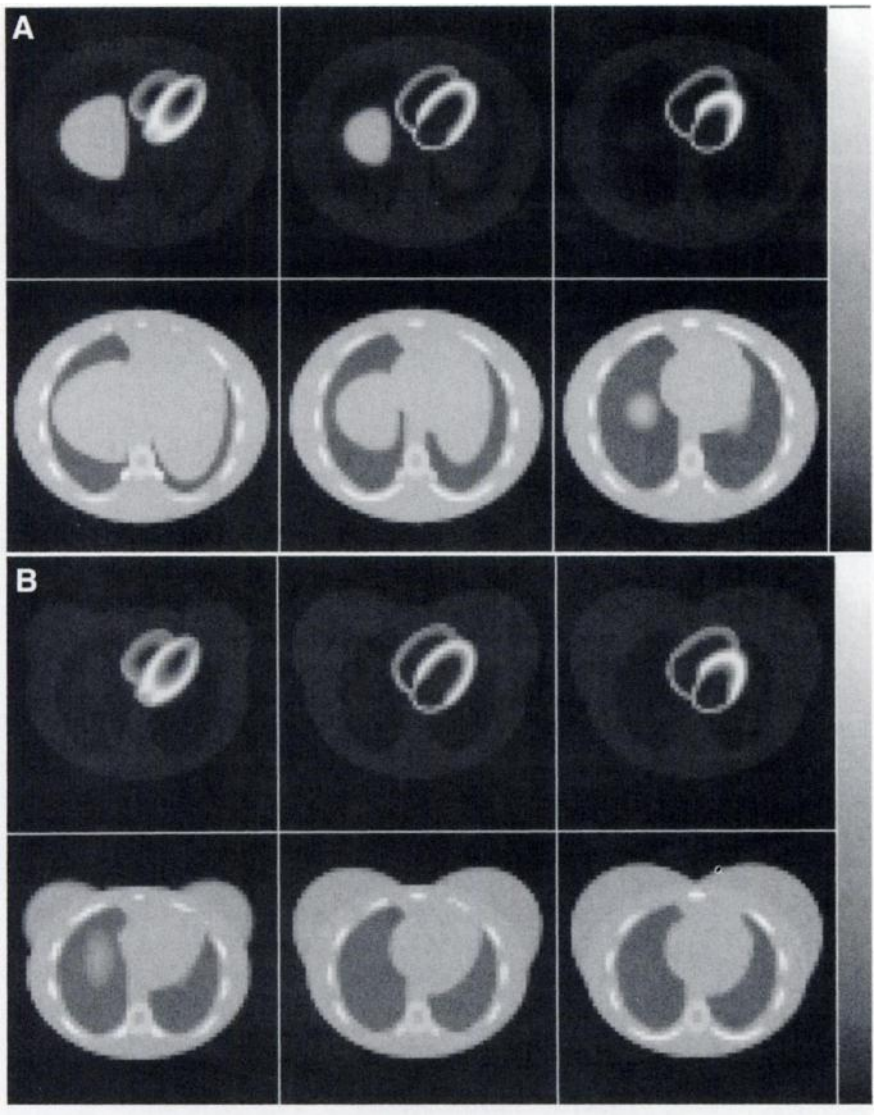

FIGURE 1. Example transaxial slices of male (A) and female (B) 3-dimensional MCAT phantoms used. Top row, ^{201}Tl emission distribution; bottom row, corresponding attenuation maps.

Truncation may be modeled in different ways in these reconstruction algorithms. In the simplest approach, the truncated bins may simply be considered to be "measured as 0." The second approach has the truncated bins modeled as having no error, i.e., the ratio of measured and estimated projection data in Equations 1 and 2 is set to 1. Finally, the truly correct way to model them is to set the appropriate terms in the projection matrix, the c_{ji} terms, to 0. We reconstructed the full set of noise realizations for the male extreme truncation case for OSEM and RBIEM at 2 views per subset using each of these 3 methods of modeling truncation. Although the first method, treating the truncated bins to be measured as 0, resulted in higher noise levels, the last 2 methods performed almost identically by quantitative measures in the heart. Because we observed the third method to give significant artifacts in the truncated region, the second method, modeling the truncated bins as having no error, was chosen for the experiments presented here.

It is important to note that there is no standard approach for modeling such truncation in clinical systems; it is purely a matter of how the reconstruction software is written. Thus, different manufacturers may use different approaches, and it is unlikely that the approach chosen will be apparent to the user. Although we believe it is reasonable to extrapolate to the other methods of modeling truncation, the results of our study apply directly to only the method we have chosen.

Analysis

From the full set of reconstructions from the 250 noise realizations, we computed the mean of each pixel, referred to as a mean image. The mean images were generated at each iteration. For quantitative evaluation, 8 ROIs were defined at anterior, lateral, inferior, and septal locations, each in both the basal and apical sections of the left ventricle. The ROIs averaged 6.0 cm^3 in volume, ranging from 4.5 to 7.3 cm^3. For each noise realization at each iteration of the algorithms, the total reconstructed image intensity in each ROI was computed. Means and variances of these ROI estimates were computed as a function of iteration. Covariances between the ROI estimates were also computed, but these showed that the totals in the different ROIs varied independently of one another and were of no particular interest.

RESULTS

Figure 2A presents the progression of mean images for the case of the male phantom with no truncation. The mean

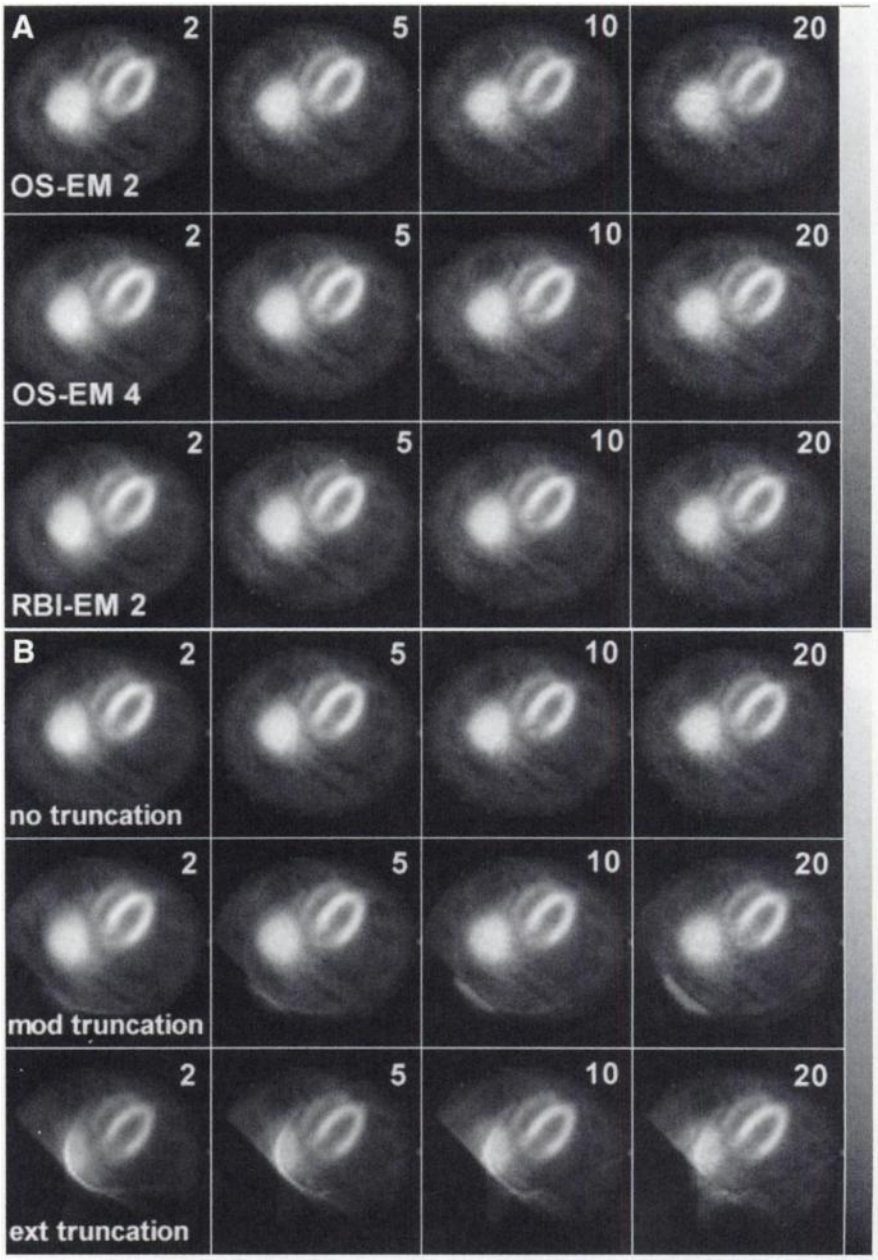

FIGURE 2. Single transaxial slice from mean images of male phantom shown at iterations 2, 5, 10, and 20. (A) Reconstruction algorithms for case of no truncation: OSEM at 2 views per subset (OSEM 2), OSEM at 4 views per subset (OSEM 4), and RBIEM at 2 views per subset (RBIEM 2). (B) Three cases of truncation: no truncation, moderate truncation, and extreme truncation for OSEM 4.

images appear to converge relatively quickly and remain unchanged after approximately 5 iterations. This supports previous evidence that, despite lacking a mathematic proof of convergence, the OSEM and RBIEM algorithms do converge in the mean (*15*). Figure 2B compares the mean images for the male phantom with OSEM at 4 views per subset as the truncation is varied. The extreme truncation case suffers from significant artifacts in the region of the truncated hot liver. The truncation of the liver is important, because it appears to affect quantitative accuracy in the basal region of the left ventricle.

Figure 3 presents a legend for the series of figures that follows. Figures 4 and 5 present the percent bias of the mean of each ROI relative to the mean for MLEM at 200 iterations with no truncation. They are therefore a measure

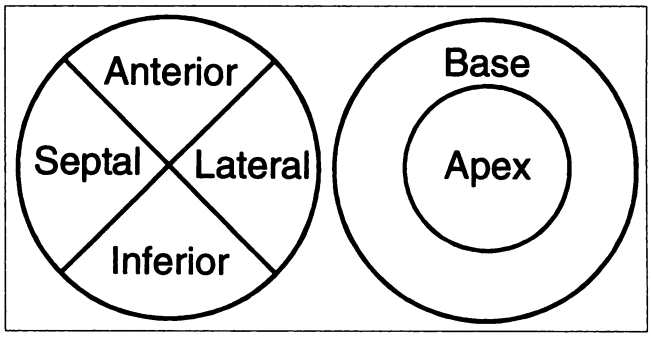

FIGURE 3. Legend for 8 regions as displayed in Figures 4 and 5.

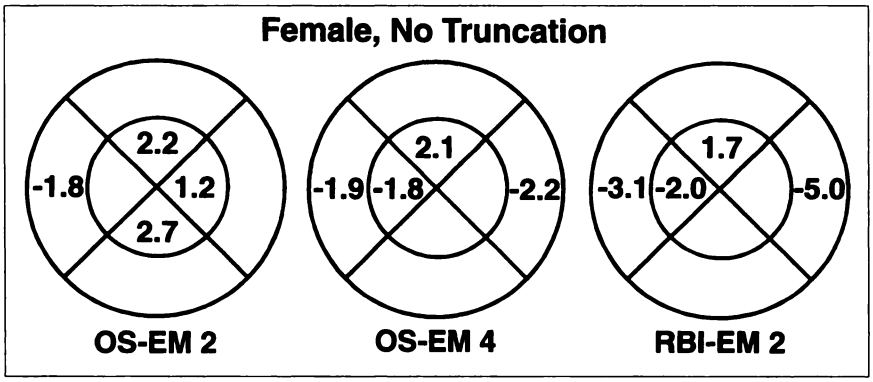

FIGURE 4. Percentage bias of each region for 3 reconstruction methods on data without truncation. Bias is computed relative to mean of MLEM algorithm at 200 iterations. Data shown are taken at 5 iterations of OSEM with 2 (OSEM 2) and 4 (OSEM 4) views per subset and RBIEM with 2 (RBIEM 2) views per subset. Biases shown were statistically significant at 95% confidence; those left blank were not significant.

of how closely the algorithms match the quantitative results of MLEM. Numbers shown in black represent a statistically significant difference from the MLEM estimate at 95% confidence. Those regions left blank had no significant difference with respect to MLEM. Significant differences were generally found for biases >1.1%, although this varied with each specific case.

Figure 4 compares the bias data for the different algorithms on the female phantom with no truncation, fixed at 5 iterations as a representative number of iterations. These data were computed relative to the MLEM results at 200 iterations, so they indicate the closeness of the algorithms in question to MLEM, on average. The percentage bias was computed as the difference between the ROI means for the 2 algorithms divided by the ROI mean for MLEM. Errors in the male phantom (not shown) were all <2.1%. Errors were somewhat higher for the female phantom, especially for RBIEM. We note, however, that the basolateral region on the female phantom was the slowest region to converge for all algorithms. Further iterations reduced the 5% error for RBIEM to within 2%. For OSEM with 4 views per subset, errors remain within 2.2% of the mean. From these data, we can conclude that, although OSEM and RBIEM do not duplicate the results of MLEM in the mean, they come very close, even on highly attenuating patients.

Figure 5 presents percentage bias data comparing results for the different levels of truncation on the male phantom for 5 iterations of OSEM with 4 views per subset. The OSEM 4 results are representative of the other algorithms, whose results are not shown. On the male phantom, we find relatively little change in going from no truncation to moderate truncation. However, significant errors result for the extreme truncation case, as high as 11% for the apicoseptal region; the effect is much smaller for the female phantom (not shown). Errors in the septal regions increase with increasing truncation but are never >3.5%. We attribute this difference in the 2 phantoms to the fact that the male phantom has a high liver that extends into the same slices as the heart, whereas the female phantom does not (Fig. 1). The activity levels simulated in the 2 livers are the same, and they suffer the same truncation, but the fact that a high-activity organ is truncated in the same slices as the heart appears to introduce significant errors in the heart itself. Variance data (not shown) for the various levels of truncation indicated that ROI variance was unaffected by truncation, even in the extreme case.

We found that, for the male phantom with extreme truncation, the MLEM errors were quite similar to those for the OSEM case, with a maximum of 11% again in the apicoseptal region. This confirms that, although considerable quantitative errors are introduced in OSEM by truncating the raised hot liver, these errors are no worse than those for MLEM under the same conditions.

To look at the effect of the number of views per subset on the variance of ROI estimates, Figure 6 plots bias versus variance for the different subset configurations. Again, only the basolateral region of the female phantom is presented, because the trends for all regions were the same. The

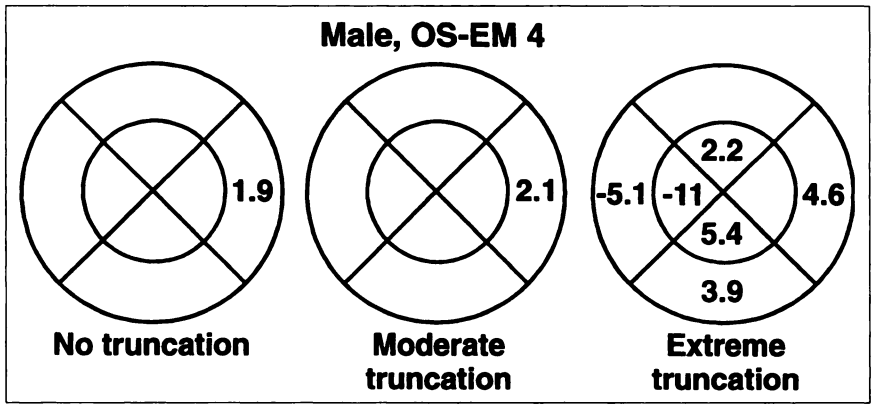

FIGURE 5. Percentage bias of each region for 5 iterations of OSEM, 4 views per subset, with different levels of truncation. Bias is computed relative to mean of MLEM algorithm at 200 iterations on data without truncation. Biases shown were statistically significant at 95% confidence; those left blank were not significant.

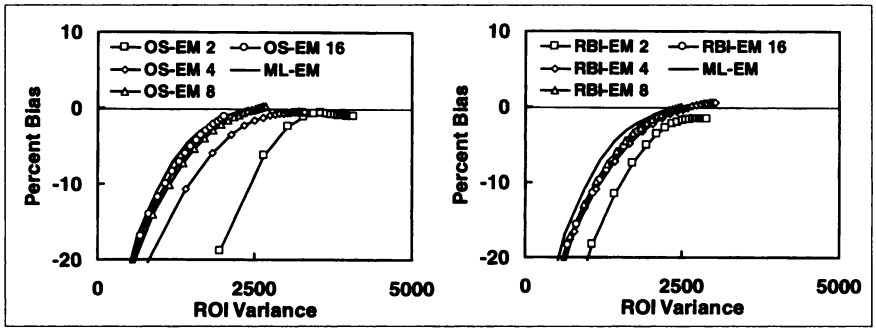

FIGURE 6. Percentage bias with respect to MLEM at 200 iterations in basolateral region for female phantom as function of variance in basolateral ROI estimate for various subset configurations. Numbers after OSEM and RBIEM indicate number of views per subset. Each marker represents 1 iteration, with iterations 1–20 going from left to right. Solid line indicates bias-variance curve for MLEM up to 200 iterations. Data are representative of relative bias-variance curves of various algorithm and subset configurations for all regions on both phantoms.

bias-variance curves for MLEM are also presented for comparison. We find a general trend that decreasing the number of views per subset moves the bias-variance curve to the right, i.e., increasing variance for a given bias. For example, for the same bias, OSEM at 2 views per subset gives a higher variance of the ROI estimate than OSEM at 4 views per subset. At 8 and 16 views per subset, the bias-variance curves for OSEM approach those for MLEM, which is, of course, OSEM with 64 views per subset. For RBIEM, the bias-variance curves are to the left of those for OSEM with the same number of views per subset; however, the RBIEM 2 curve follows almost the identical track of OSEM 4. The same is true comparing RBIEM 4 with OSEM 8, and so on. Thus, we can achieve almost identical performance between OSEM and RBIEM by varying the number of views per subset. This result expands on our previous paper (*15*), in which we compared the 2 with the same number of views per subset. In that article, we concluded that OSEM was faster and had higher image noise, but we did not examine the effects of changing the subset configurations.

Finally, in Figure 7, we summarize the magnitudes of the various sources of error for the female phantom at likely operating points for iteration number as we change the number of views per subset. The iteration numbers were chosen on the basis of the relative convergence rates of the ROI means of the various algorithms. The errors shown represent the bias with respect to MLEM at 200 iterations, the bias with respect to the true phantom, and 1 SD of the ROI estimate. The bias with respect to the true phantom was computed by normalizing all values to the average of the 8 ROIs, so it represents a measure of relative and not absolute quantitative accuracy. The values shown are the maximum errors over the 8 regions for each case and may represent errors in different regions.

The measures shown in Figure 7 represent 2 potential sources of misdiagnosis, because they represent errors that may be encountered in scoring segments of the left ventricle. The bias with respect to the true phantom indicates the error inherent in the system, including the data acquisition and reconstruction processes, when no noise is present. The SD indicates the magnitude of the statistical variation in the intensity of individual ROIs or cardiac segments and represents errors resulting simply from the random nature of data acquisition.

In Figure 7, we first note that the biases with respect to MLEM at 200 iterations are small compared with both the

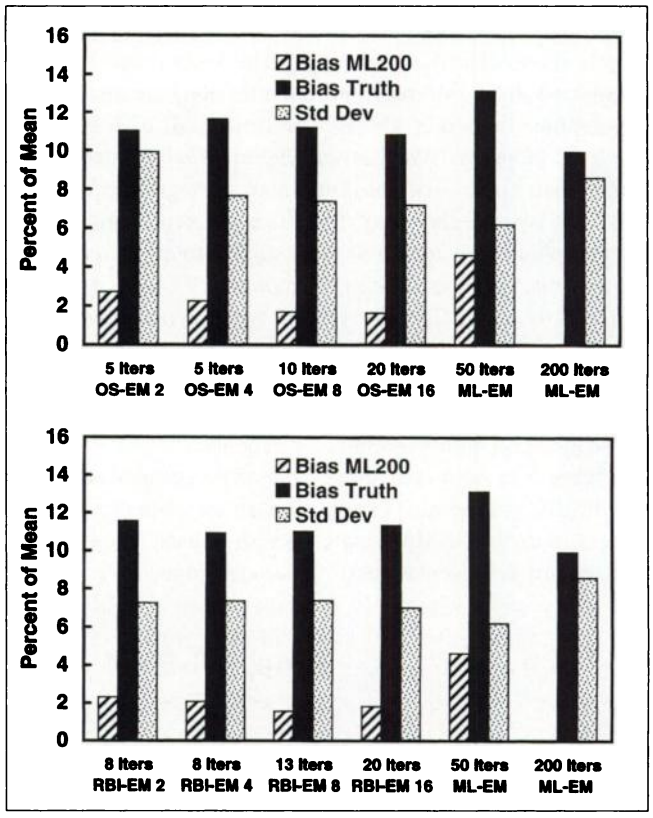

FIGURE 7. Maximum errors over all 8 regions as percentage of mean for various algorithm and subset configurations at likely operating points for iteration number. Data shown are for female phantom; similar trends were observed for male phantom. Errors shown are bias with respect to MLEM at 200 iterations (Bias ML200), bias with respect to true phantom (Bias Truth), and 1 SD (Std Dev) of ROI estimate. Numbers after OSEM and RBIEM indicate number of views per subset.

biases with respect to the true phantom and the SDs. Thus, even though they are statistically significant in many cases, they are well below the inherent error with respect to the truth and variations resulting from noise. The bias with respect to the true phantom has the greatest magnitude of error in all cases. We attribute this to errors resulting from scatter and to the limited spatial resolution of the system. To check the effect of scatter, we performed a similar study on the female phantom using scatter compensation (*22*) and found that the maximum errors with respect to the true phantom were reduced by 4%, bringing them down to the level of a single SD.

With the exception of OSEM 2, all iteration numbers chosen exhibited similar errors with respect to truth and similar SDs. In general, the performance of these iteration numbers was close to that from MLEM at approximately 100 iterations. OSEM 2 exhibited a significantly higher SD for approximately the same level of bias, consistent with the bias-variance curves shown in Figure 6.

DISCUSSION

We find that the OSEM and RBIEM algorithms give reconstructions that are very close on average, though not identical, to those from the MLEM algorithm. This is true even under the extreme conditions of attenuation and truncation examined here. The algorithms clearly require far fewer iterations to reach nearly the same estimate. This observation is important, because it helps to justify the use of OSEM and RBIEM, despite the fact that they lack proof of convergence. When examining the ROI variances, however, we find that the subset configuration can have a significant effect on the image noise level and consequently on the variation in regional quantitative estimates. That variation can lead to errors in determining the relative perfusion of a section of myocardium in borderline cases; thus, to reduce it as much as possible is important.

As the number of views per subset is decreased, the number of iterations to reach a certain level of bias is decreased. There is a price to be paid for increased speed, in that the image noise will increase for the same level of bias. Thus, the use of OSEM with 2 views per subset should be discouraged because of the prodigious increase in noise (Figs. 6 and 7). OSEM with 4 views per subset and RBIEM with 2 views per subset also exhibit slightly worse bias-variance tradeoffs than slower configurations with more views per subset, but that must be considered in light of the time required to reconstruct the data. In a clinical environment, the reconstructed images will be as good as or better than unreconstructed images if fewer subsets and more iterations are used, but this will require additional processing time. The optimal choice will depend on the conditions in a given clinic, including the speed of the reconstruction computer and the desired time from patient measurement to presentation of the images to the nuclear medicine physician.

The RBIEM algorithm was found to perform very similarly to OSEM when OSEM used twice the number of views per subset as RBIEM. In the past, we have observed that RBIEM exhibited lower noise than OSEM at the same iteration number (*15*), but those comparisons were done for the same subset configuration. In addition, we have speculated that, because RBIEM can be shown to converge to the ML solution for consistent data (*14*), it may have better convergence properties. From this work, however, we note that OSEM can be made to perform similarly to RBIEM simply by adjusting the subset configuration. Thus, there is probably no advantage or disadvantage to using OSEM as opposed to RBIEM. Because RBIEM is less well known, it is likely that OSEM will remain the dominant iterative reconstruction algorithm in the field.

Several items that may affect the application of OS algorithms were not considered in this study and should be examined. First, noiseless attenuation maps were used in all cases. Attenuation maps obtained from clinical systems are noisy, and the effects of noise in attenuation maps have not been studied for ordered-subset reconstructions. Second, our simulation assumes a stationary patient, but patient motion can be a significant source of artifacts. This is especially important with OS methods, because the timing of voluntary patient motion and the method by which the subsets are grouped may determine the severity of motion artifacts in the reconstruction.

CONCLUSION

The OSEM and RBIEM algorithms are adequate substitutes for MLEM in myocardial perfusion SPECT, giving similar quantitative results in the mean, even in extreme cases of attenuation and truncation. Unacceptable errors do result from truncation of high-activity organs in the same slices as the heart, but these are no worse for OSEM and RBIEM than for MLEM. This indicates that such extreme truncation should be avoided no matter what reconstruction algorithm is used. The number of views per subset, or alternately the number of subsets, is significant in determining the number of iterations required for regional quantitative estimates to converge. Increasing the number of subsets decreases the number of iterations required to reach a certain point of convergence and, thus, the total reconstruction processing time; however, increasing the number of subsets will increase reconstructed image noise. We recommend that OSEM not be used with fewer than 4 views per subset to avoid significant increases in image noise. We also recommend that clinical users consider using the fewest subsets possible with regard to the processing time available.

ACKNOWLEDGMENT

This work was supported by grant CA 39463 from the U.S. National Cancer Institute. Its contents are solely the responsibility of the authors and do not necessarily represent the official views of the National Cancer Institute.

REFERENCES

1. Malko JA, Van Heertum RL, Gullberg GT, Kowalsky WP. SPECT liver imaging using an iterative attenuation correction algorithm and an external flood source. *J Nucl Med.* 1986;27:701–705.
2. Manglos SH, Thomas FD, Capone RB. Attenuation compensation of cone beam SPECT images using maximum likelihood reconstruction. *IEEE Trans Med Imaging.* 1991;10:66–73.
3. Tsui BMW, Gullberg GT, Edgerton ER, et al. Correction of nonuniform attenuation in cardiac SPECT imaging. *J Nucl Med.* 1989;30:497–507.
4. Lange K, Carson R. EM reconstruction algorithms for emission and transmission tomography. *J Comp Assist Tomogr.* 1984;8:306–316.
5. Shepp LA, Vardi Y. Maximum likelihood estimation for emission tomography. *IEEE Trans Med Imaging.* 1982;1:113–121.
6. Barrett HH, Wilson DW, Tsui BMW. Noise properties of the EM algorithm: part I. Theory. *Phys Med Biol.* 1994;39:833–846.
7. Chornoboy ES, Chen CJ, Miller MI, Miller TR, Snyder DL. An evaluation of maximum likelihood reconstruction for SPECT. *IEEE Trans Med Imaging.* 1990; 9:99–110.
8. Gooley TA, Barrett HH. Evaluation of statistical methods of image reconstruction through ROC analysis. *IEEE Trans Med Imaging.* 1992;11:276–283.
9. Liow J-S, Strother SC. Practical tradeoffs between noise, quantitation, and number of iterations for maximum likelihood-based reconstructions. *IEEE Trans Med Imaging.* 1991;10:563–571.
10. Miller TR, Wallis JW. Clinically important characteristics of maximum-likelihood reconstruction. *J Nucl Med.* 1992;33:1678–1684.
11. Snyder DL, Miller MI, Thomas LJ Jr, Politte DG. Noise and edge artifacts in maximum likelihood reconstruction for emission tomography. *IEEE Trans Med Imaging.* 1987;6:228–238.
12. Wilson DW, Tsui BMW, Barrett HH. Noise properties of the EM algorithm: part II. Monte Carlo simulations. *Phys Med Biol.* 1994;39:847–871.
13. Hudson HM, Larkin RS. Accelerated image reconstruction using ordered subsets of projection data. *IEEE Trans Med Imaging.* 1994;13:601–609.
14. Byrne CL. Block-iterative methods for image reconstruction from projections. *IEEE Trans Imag Proc.* 1996;5:792–794.
15. Lalush DS, Tsui BMW. Mean-variance analysis of block-iterative reconstruction algorithms modeling 3D detector response in SPECT. *IEEE Trans Nucl Sci.* 1998;45:1280–1287.
16. Tsui BMW, Hu H, Gilland DR, Gullberg GT. Implementation of simultaneous attenuation and detector response correction in SPECT. *IEEE Trans Nucl Sci.* 1988;35:778–783.
17. Zeng GL, Gullberg GT. Frequency domain implementation of the three-dimensional geometric point response correction in SPECT imaging. In: *Conference Record of the 1991 IEEE Nuclear Science Symposium and Medical Imaging Conference, Santa Fe, NM, 2–9 November 1991.* Piscataway, NJ: Institute of Electrical and Electronic Engineers; 1991:1943–1947.
18. Frey EC, Ju ZW, Tsui BMW. A fast projector-backprojector pair for modeling the asymmetric spatially-varying scatter response function for scatter compensation in SPECT imaging. *IEEE Trans Nucl Sci.* 1993;40:1192–1197.
19. Beekman F, Kamphuis C, Viergever M. Improved SPECT quantitation using fully three-dimensional iterative spatially variant scatter response compensation. *IEEE Trans Med Imaging.* 1996;15:491–499.
20. Tsui BMW, Terry JA, Gullberg GT. Evaluation of cardiac cone-beam single photon emission computed tomography using observer performance experiments and receiver operating characteristic analysis. *Invest Radiol.* 1993;28:1101–1112.
21. LaCroix KJ. *Evaluation of an Attenuation Compensation Method with Respect to Defect Detection in Tc-99m-MIBI Myocardial SPECT Images* [dissertation]. Chapel Hill, NC: The University of North Carolina at Chapel Hill; 1997.
22. Kadrmas DJ, Frey EC, Karimi SS, Tsui BMW. Fast implementations of reconstruction-based scatter compensation in fully 3D SPECT image reconstruction. *Phys Med Biol.* 1998;43:857–874.